

Supplementary Information

Dynamic viscosity mapping of the oxidation of squalene aerosol particles.

Athanasios Athanasiadis,^{a†} Clare Fitzgerald,^{b†} Nicholas M. Davidson,^c Chiara Giorio,^b Stanley W. Botchway,^d Andrew D. Ward,^d Markus Kalberer,^{b*} Francis D. Pope^{c*} and Marina K. Kuimova^{a*}

^a Department of Chemistry, Imperial College London, London, SW7 2AZ, UK.

E-mail: m.kuimova@imperial.ac.uk

^b Department of Chemistry, University of Cambridge, Cambridge, CB2 1EW, UK.

E-mail: markus.kalberer@atm.ch.cam.ac.uk

^c School of Geography, Earth and Environmental Science, University of Birmingham, Edgbaston, B15 2TT, UK. E-mail: f.pope@bham.ac.uk

^d Central Laser Facility, Rutherford Appleton Laboratory, Chilton, Didcot, Oxon OX11 0QX, UK.

Contents

Contents:	1
A. The molecular structure of squalene	2
B. Calibration of Bodipy-C10	3
C. Control test of exposure of squalane/Bodipy-C10 droplets to ozone	4
D. Squalene oxidation products	5
E. The phase test of Squalene particle following complete oxidation with ozone	8
F. The goodness of fit (χ^2) values for Squalene/Bodipy-C10 particle oxidation	9
G. Raman spectroscopy of a trapped squalene droplet recorded during oxidation with ozone ... 10	
H. Hydroxyl radical detection using HPF	11
I. Change in viscosity of suspended squalene aerosol with exposure to hydroxyl radicals	13
J. Comparison of oxidation products between ozonolysis and oxidation by OH radicals	15
K. Brightfield images of \cdotOH oxidised squalene/Bodipy-C10 particles	16
L. Effect of oxidant gases on squalene aerosol	17
M. Absorption spectrum of squalene	19
N. Effect of FLIM laser exposure on the fluorescence lifetime	20
O. References	21

A. The molecular structure of squalene

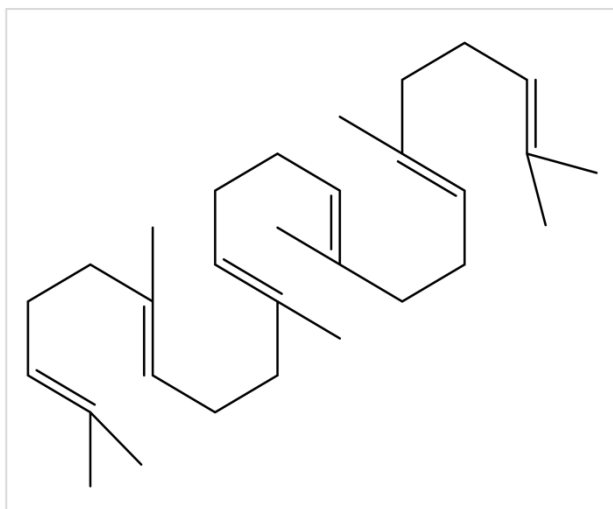


Fig. S1. The molecular structure of squalene

B. Calibration of Bodipy-C10

The Bodipy-C₁₀ calibration curve was measured earlier^{1,2} in methanol/glycerol mixtures of increasing viscosity and should conform to the Förster-Hoffmann equation³, namely

$$\log \tau_f = \log \frac{z}{k_r} + \alpha \log \eta$$

where τ_f is the fluorescence lifetime, η viscosity, k_r radiative decay rate and α , z constants.

This equation works well for Bodipy-C₁₀ between 15 and 1000 mPa s.⁴ However, at higher viscosity values, as the maximum quantum yield for the rotor is approached, the linearity between the $\log \tau_f$ and $\log \eta$ was lost (Fig. S2)^{2,1}. Thus, in the range of lifetimes exceeding 5 ns, a very small change in fluorescence lifetime corresponds to a large change in viscosity.

In order to estimate the maximum fluorescence lifetime expected for Bodipy-C₁₀ when completely immobilised, we have measured the fluorescence decay of Bodipy-C₁₀ embedded in the glassy matrix of ethanol-methanol ($\eta=2 \times 10^{14}$ mPa s) and 2-Methyltetrahydrofuran ($\eta=4 \times 10^9$ mPa s) at 77 K. We find that the decays can be well fitted with a monoexponential function (Fig. S2A) and the lifetime values were 6.0 and 5.7 ns, respectively. We therefore assume that ca 6 ns is the limiting fluorescence lifetime value for Bodipy-C₁₀ lifetime at the highest viscosity.

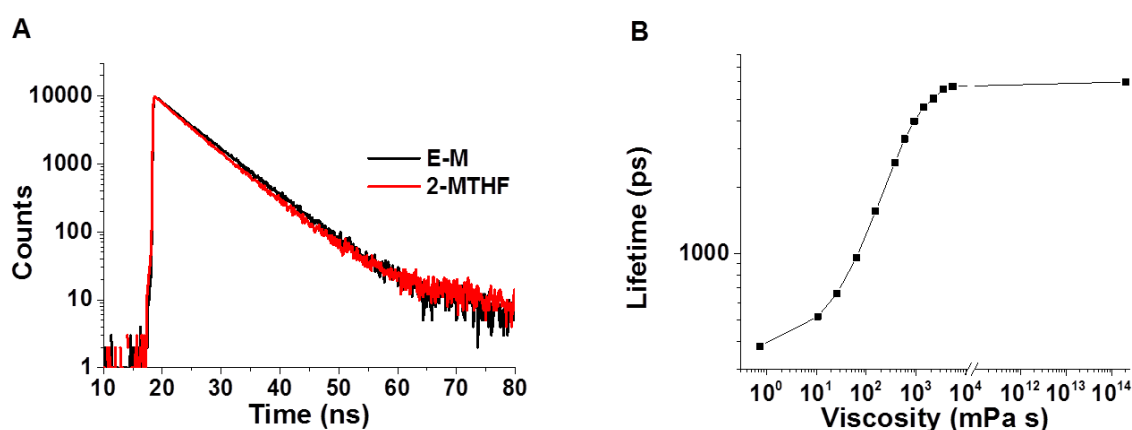


Fig. S2. (a) Fluorescence decays of Bodipy-C₁₀ in glassy ethanol-methanol (E-M) ($\eta=2 \times 10^{14}$ mPa s) and 2-Methyltetrahydrofuran (2-MTHF) ($\eta=4 \times 10^9$ mPa s) matrices, with fluorescent lifetimes of 6.0 and 5.7 ns respectively, and (b) the calibration of Bodipy-C₁₀ in the Förster-Hoffmann equation coordinates.

C. Control test of exposure of squalane/Bodipy-C10 droplets to ozone

A test was carried out to see whether the exposure to ozone would affect the lifetime of the Bodipy-C₁₀ rotor. Bodipy-C₁₀, dissolved in neat squalane (99%, Sigma Aldrich), was exposed to ozone and the fluorescence lifetime measured. Squalane was chosen as the solvent since it contains no double bonds and therefore could be assumed to not react with ozone. The dye/squalane mixture was nebulised onto a slide and exposed to an ozone flow. The fluorescence lifetime of the droplets was measured over the time range of the oxidation experiments. The measurements were recorded for 868 and 377 ppm of ozone. Fig. S3 shows that an increase in lifetime was measured due to ozone exposure of ~ 1 ns after 700 s exposure to 868 ppm O₃. Therefore there is a reaction occurring between the dye and the ozone, resulting in either a by-product with a longer lifetime or an increase in the viscosity of the droplet. However, this change in lifetime was significantly less than that observed in the alkene ozonolysis and may be attributable to the effect of prolonged laser exposure (see discussion below).

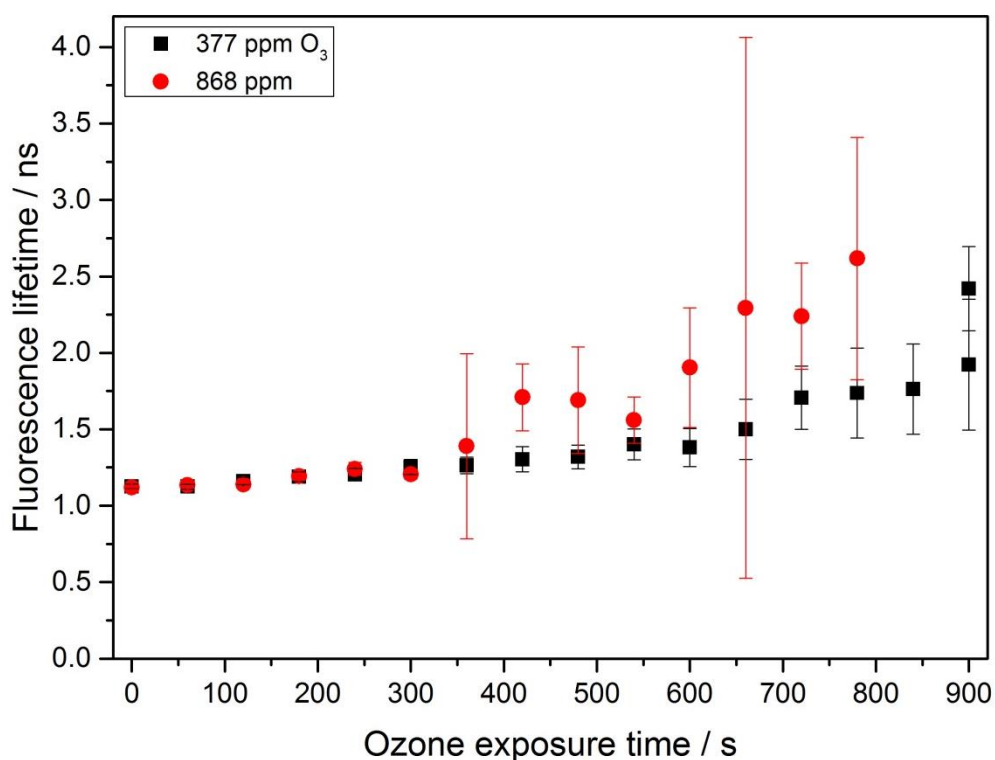


Fig. S3. Effect of ozone on the fluorescence lifetime of Bodipy-C₁₀ dye dissolved in squalane droplets. Black squares: 377 ppm ozone concentration; red circles: 868 ppm. Note that no physical changes were observed in the droplet's viscosity or morphology following the exposure to 53 ppm of ozone (equivalent to what was used for squalene oxidation in this work).

D. Squalene oxidation products

Liquid extraction surface analysis-mass spectrometry (LESA-MS) was used to characterise the products of squalene ozonolysis. The mass spectra helped to identify at a molecular level what induces a viscosity increase.

LESA-MS analyses were done on oxidised slides of squalene after ozonolysis as well as after reaction with $\cdot\text{OH}$. This is a useful technique which allows the surface of a sample to be analysed by mass spectrometry without complicated sample processing ⁵. A solvent mixture is required that the sample will be soluble in and the LESA method extracts the sample from the surface by depositing droplets of the solvent onto the sample. This creates a solvent/sample solution that can be sprayed into the mass spectrometer.

Oxidised squalene samples were prepared as for the surface FLIM experiments, i.e. nebulised aerosol on a cover-slide and then 50 minutes of ozonolysis reaction or 70 minutes reaction with $\cdot\text{OH}$. It is likely that larger droplets on the slide would not have fully reacted in this time and some starting material would have been present in the oxidised mixture. However, due to the ionisation mechanism (ESI) used in the mass spectrometry analysis, the squalene molecular ion would not have been seen in the mass spectra, as it does not readily deprotonate to form a negative ion.

An acetonitrile-water (90:10) mixture was used for the sample extraction from the slide. To increase spray stability and ionisation efficiency, 0.1% formic acid was added to the water in the solvent mixture ⁶. Three microlitres of solvent were deposited at a height of 0.8 mm from the sample plate at the maximum dispensation rate ($60 \mu\text{L min}^{-1}$). The liquid junction was maintained for 25 s. The droplets containing the dissolved analytes were then aspirated at a height of 0.6 mm from the sample plate and infused in a chip-based nanoESI source (Triversa NanoMate Advion, Ithaca, USA). Blanks were analysed by repeating the same procedure on organic droplets before oxidation. The ultrahigh-resolution mass spectrometer (LTQ Orbitrap Velos Mass spectrometer (Thermo Scientific)) was used to analyse the organic compounds present in the samples following extraction. Samples were sprayed at a gas (N_2) pressure of 0.8 psi at -1.2 kV in negative ionisation mode, with a transfer capillary temperature of 210 °C. Data were acquired using an automated acquisition method to measure the full scan in the m/z ranges 100-600, 150-1000 and 400-2000. For each droplet, a minimum of 15 scan routines were acquired (~1.5 minutes of acquisition).

Fig. S4 shows the mass spectra for the products of squalene ozonolysis in the m/z range 100-200 and 200-2000. The molecular weight of squalene is 410 g mol^{-1} . The mass spectra show that there are products formed of lower and higher molecular weight than the starting compound.

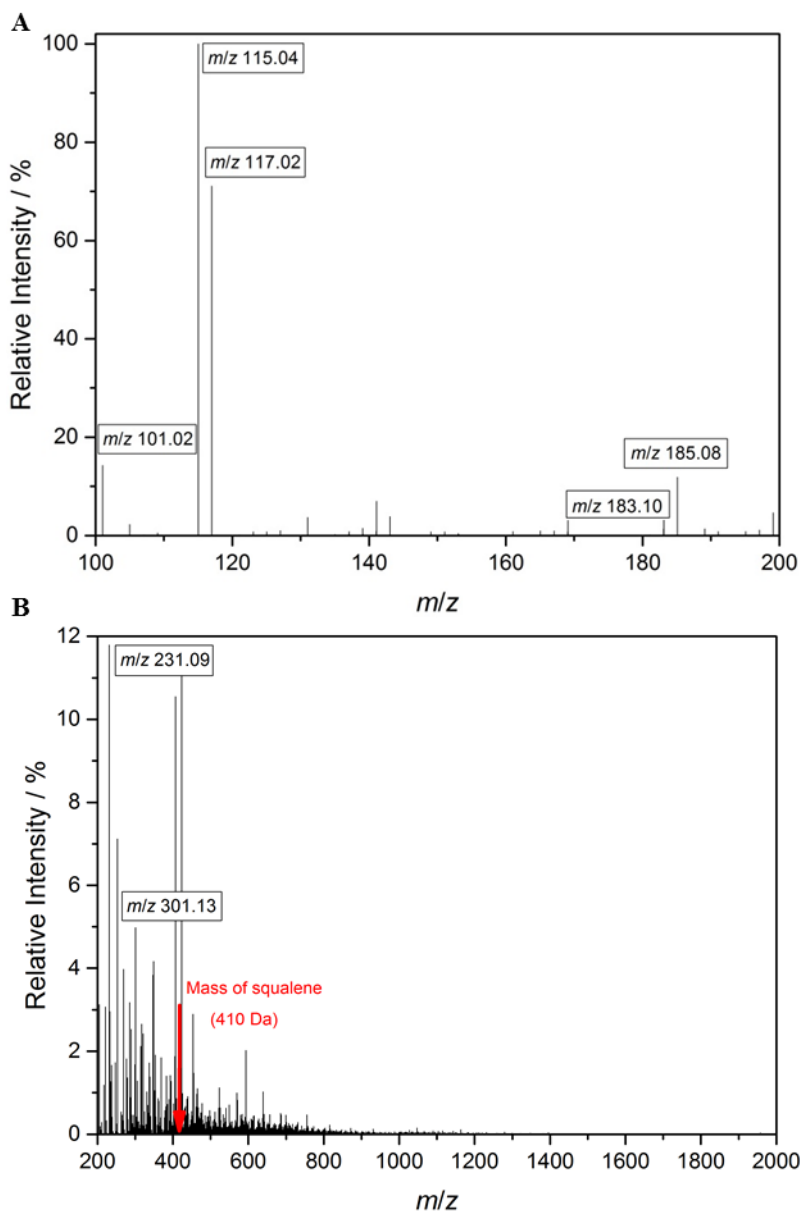


Fig S4. Mass spectra for products of squalene ozonolysis: A: m/z 100-200, B: Higher mass region m/z 200-2000. Peaks are labelled and characterised in Table S1 and Table S2.

Examples of ozonolysis products are listed in Table S1. Although these molecules are smaller than the starting compound squalene, they are highly oxidised, containing a mixture of aldehyde and carboxylic acid functional groups. Therefore the degree of dipole-dipole interactions between molecules will have increased within the mixture after oxidation.

Listed in Table S2 are tentatively assigned example secondary products that form from addition of the monomers to a CI and each other. The examples included in the tables were structures that could be easily deduced from the characteristic ozonolysis reaction pathways, although it can be seen from the mass spectra that a large variety of compounds are produced, emphasising the complexity of these reactions. These molecules will be bulkier than the monomer compounds and more oxidised. Both factors will have contributed to the measured increase in viscosity.

Table S1. Example monomer products from the ozonolysis of squalene, detected using mass spectrometry.

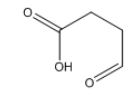
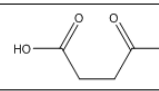
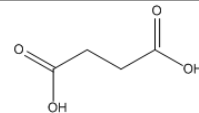
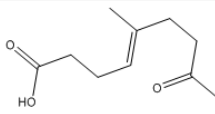
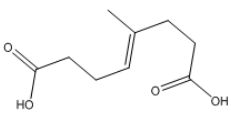
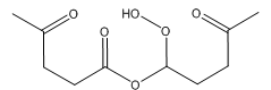
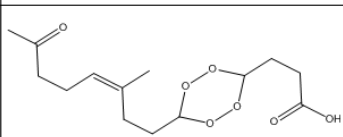
	<i>m/z</i> (deprotonated)	Relative Intensity %	Composition (neutral)	Possible Monomers	Oxygenated Functional groups	Proposed Structure
Monomers	101.02	14.30	C ₄ H ₆ O ₃	M2 reaction with water (solvent)	Carboxylic acid, aldehyde	
	115.04	100.0	C ₅ H ₇ O ₃	M1	Carboxylic acid, ketone	
	117.02	71.10	C ₄ H ₆ O ₄	M2	Carboxylic acid	
	183.1	3.10	C ₁₀ H ₁₆ O ₃	M3	Carboxylic acid, ketone	
	185.08	11.90	C ₉ H ₁₄ O ₄	M4	Carboxylic acid	

Table S2. Example dimer products from the ozonolysis of squalene, detected using mass spectrometry.

	<i>m/z</i> (deprotonated)	Relative Intensity %	Composition (neutral)	Possible Monomers	Linker functional group	Proposed Structure
Dimers	231.09	11.70	C ₁₀ H ₁₆ O ₆	2 x M1	α -hydroxyalkyl peroxide	
	233.07	2.40	C ₉ H ₁₄ O ₇	M1 + M2	diperoxide	
	301.13	4.30	C ₁₄ H ₂₂ O ₇	M2 + M3	diperoxide	

E. The phase test of Squalene particle following complete oxidation with ozone

It could not be definitively concluded from the cover slide FLIM measurements whether solidification was also occurring on the slide, due to a different optical setup being used for these measurements as well as a possible change in geometry of a droplet itself. To test for solidification of droplets after ozonolysis, the cover-slide was scraped with a pipette tip to see the response of the droplets. This was analogous to the 'Poke-flow' technique designed by Renbaum-Wolff et al. (2013).⁷

Figure S5 shows the fluorescence intensity image of a scraped droplet. It appears to have smudged rather than shattered, the latter expected from a solid particle. Therefore, at most the ozonolysed squalene on the slide is a high viscosity liquid, whereas there is evidence (Figure 1 and Figure 3) that the trapped particles are solidifying.

It is possible that, in the absence of contact with a surface, alongside analysing smaller particle sizes, smaller, more volatile oxidation products, such as aldehydes, partition more readily into the gas phase from the trapped oxidised particle. This would potentially result in a more viscous aerosol consisting of heavier molecular weight products.

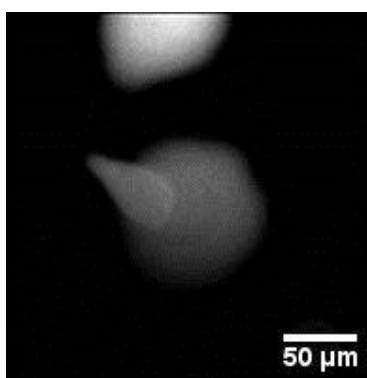


Fig. S5. Fluorescence intensity image of an ozonised squalene droplet after being scraped to infer its phase.

F. The goodness of fit (χ^2) values for Squalene/Bodipy-C10 particle oxidation

The Bodipy-C₁₀ molecular rotor is characterised by monoexponential excited state decays, if it is placed in a homogeneous environment. Indeed, the FLIM images of the trapped squalene droplets recorded at early stages of ozonolysis can be fitted using monoexponential decay function with acceptable goodness of fit values (χ^2), as shown below.

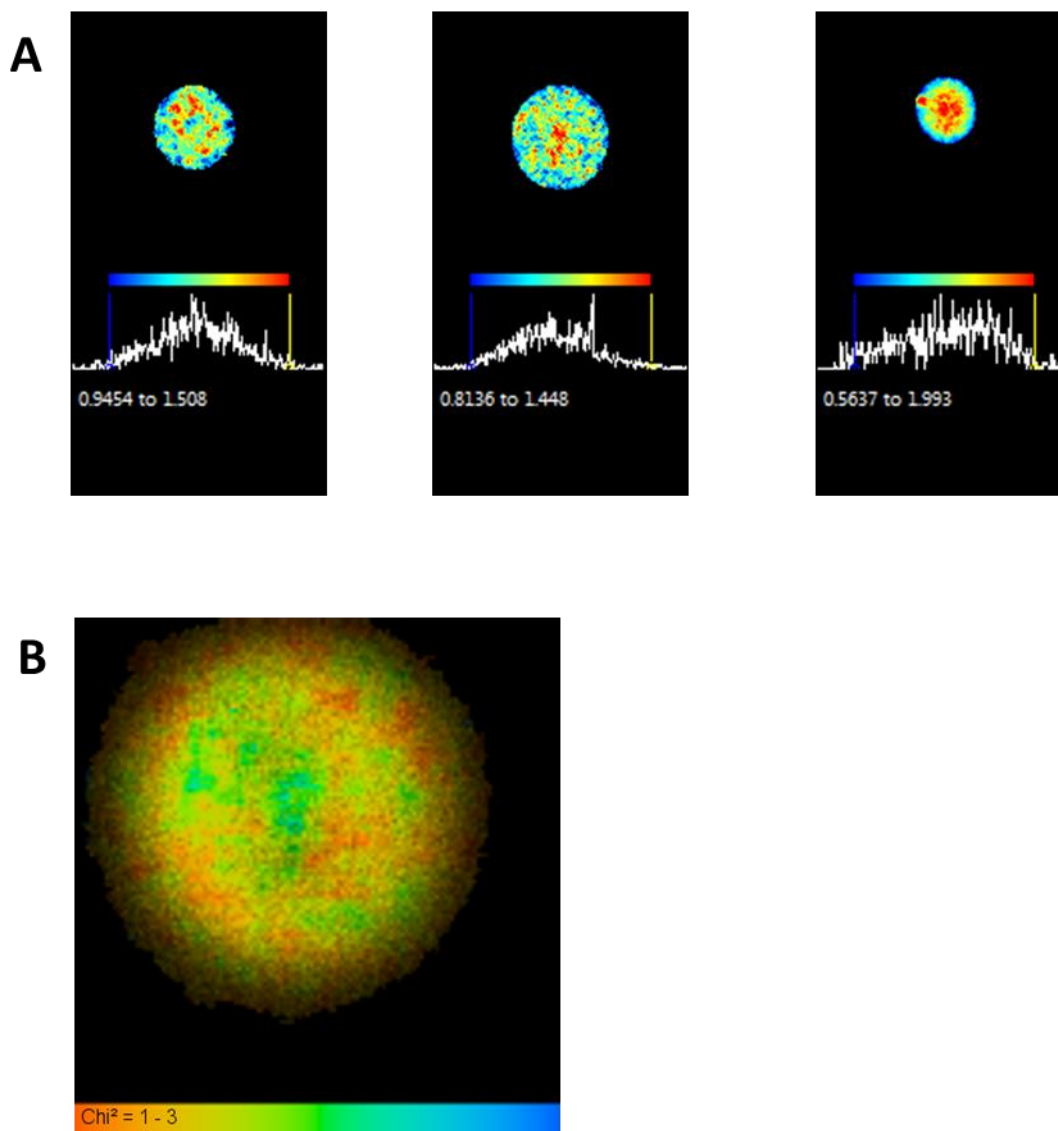


Fig. S6. (A) Goodness of fit (χ^2) images of three individual squalene/Bodipy-C10 droplets before oxidation. (B) (χ^2) image of the droplet shown in Figure 3, for lifetime fitted with a floating scatter.

G. Raman spectroscopy of a trapped squalene droplet recorded during oxidation with ozone

To investigate the chemistry of the trapped squalene particle undergoing ozonolysis (ozone concentration = 11 ppm), a complimentary experiment was performed using a similar optical trap configured with Raman spectroscopic probe. Figure S7 provides normalised spectra of the squalene particle before, during and after ozonolysis. Since the intensity of Raman scattering is proportional to the square of the polarisability of any given bond, the addition of the strongly electronegative oxygen, that occurs upon ozonolysis, to an organic molecule draws electron density towards the oxygen atom, thus reducing the mobility of all adjacent bonds and significantly reducing the Raman signal intensity from the sample as a whole, which was indeed observed in our data. To account for the change in Raman signal intensity, the Raman signal was normalised against a C-H symmetric deformation stretching band at 1390 cm^{-1} - a bond type that is not directly influenced by the ozonolysis reaction. The normalized spectra reveal the expected chemistry of ozonolysis of C=C double bonds. In particular, the fall in the C=C peak at 1620 cm^{-1} can be seen relative to the rest of the signal. The addition of oxygen to the particle can be observed as a generation of carbonyl bonds and peroxide bonds at 1682 cm^{-1} and 818 cm^{-1} , respectively.

There are also clear changes in the C-H finger print region ($2700\text{-}3200\text{ cm}^{-1}$). The loss of distinction of the C-H twisting and wagging modes in the $1200\text{-}1400\text{ cm}^{-1}$ region likely illustrates the loss of mobility of adjacent bonds post-ozonolysis, although the relative stability of the stretching modes in the fingerprint region shows that the bonds remain intact.

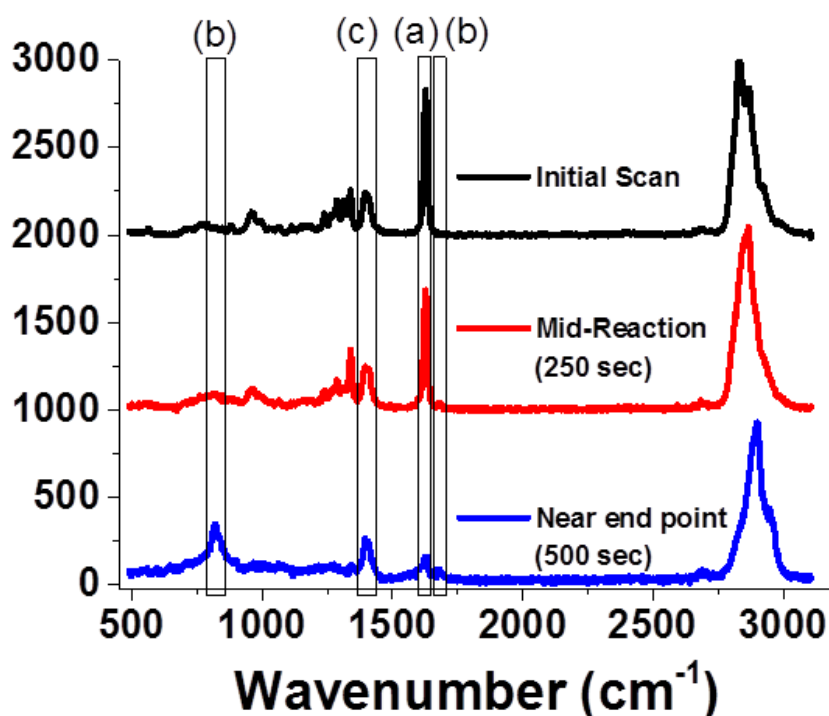


Fig. S7. The Raman spectra of a trapped $10\mu\text{m}$ droplet of squalene under exposure to $200\text{cm}^3/\text{min}$ of oxygen with 11ppm of ozone generated by a penray lamp. The distinctive C=C stretch at 1620cm^{-1} (a) is reduced as the ozone breaks the double bonds in the squalene molecules. At the same time, an organic peroxide peak at 818cm^{-1} and a C=O stretch at 1682cm^{-1} (b) become more pronounced as the reaction proceeds. All spectra are normalised against the C-H stretch at 1390cm^{-1} (c).

H. Hydroxyl radical detection using HPF

A qualitative fluorescence based detection method was used to confirm that OH radicals were reaching the sample chamber, as it was possible that by the time the vapour reached the sample, very few radicals remained, since the lifetime of $\cdot\text{OH}$ before they recombine to form H_2O_2 is very short (<1 s), alongside other losses such as deposition on the tubing and chamber walls.

The compound 3'-(p-hydroxyphenyl) fluorescein (HPF, Sigma Aldrich) was used. HPF is a fluorescent probe developed by Setsukinai et al for the selective detection of $\cdot\text{OH}$ or hypophalites. It selectively reacts with the OH radical to form a fluorescein molecule which is strongly emissive (Fig. S8)⁸. It is also shown not to react with other reactive oxygen species such as $\text{O}_2^{\cdot-}$, $^1\text{O}_2$ and H_2O_2 .

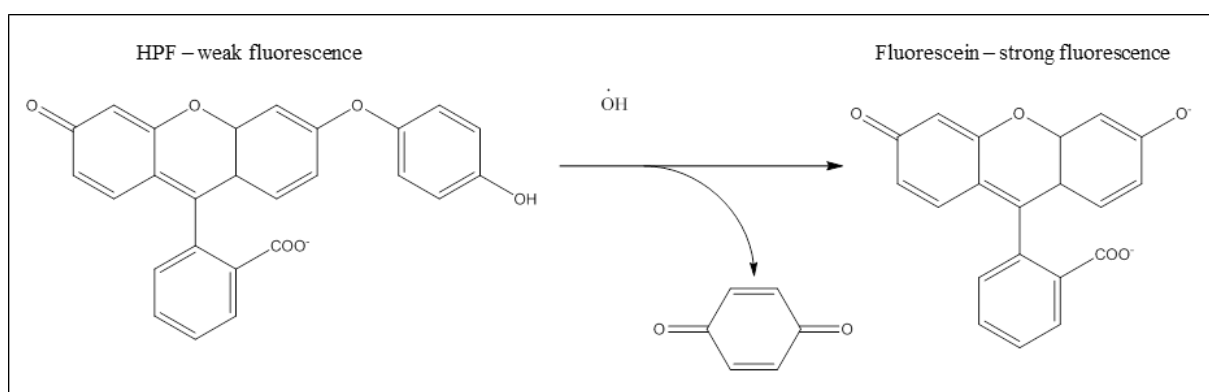


Fig. S8. Structure of HPF molecule and fluorescein product after reaction with $\cdot\text{OH}$.

To test if $\cdot\text{OH}$ were reaching the sample chamber, a droplet of HPF in water ($5\ \mu\text{M}$) was placed on the bottom cover-slide of the chamber and the oxidant gas flow was passed over the droplet. Single fluorescence decays of the droplet were taken continuously to observe whether an increased intensity was detected, which would be attributed to formation of fluorescein due to reaction with $\cdot\text{OH}$. Fig S9 shows the measured increase in fluorescence intensity, using the amplitudes of each decay. The measured increase in the decay amplitude from ~ 120 -550, confirms that $\cdot\text{OH}$ can be produced by the H_2O_2 vapour plus photolysis and that they reach the sample chamber.

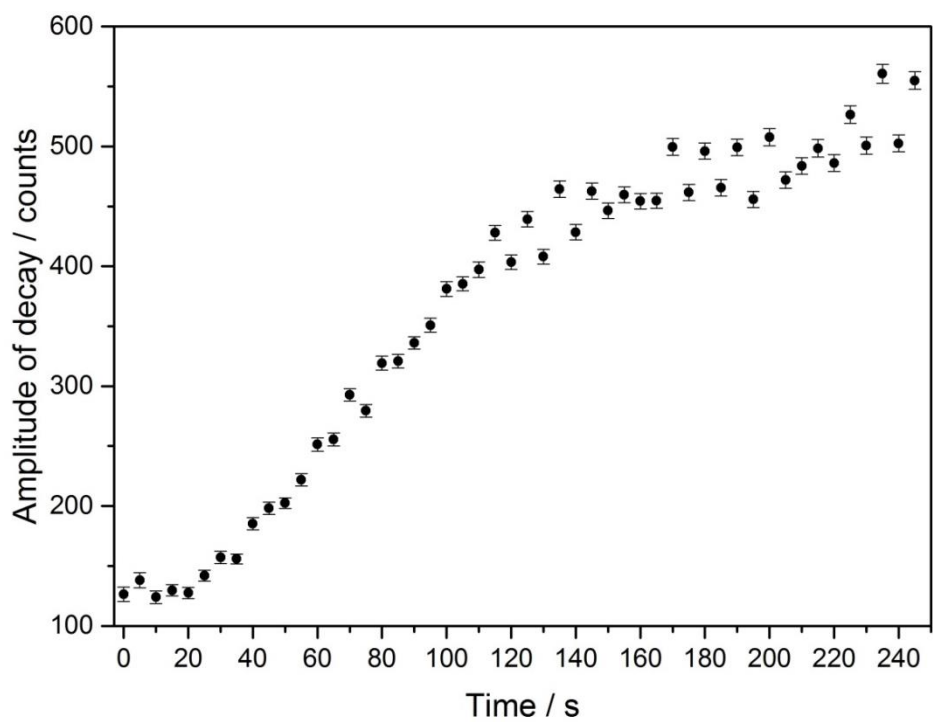


Fig. S9. Increase in fluorescence intensity upon exposure of an aqueous HPF droplets to $\cdot\text{OH}$ produced in our setup. The intensity increase follows the formation of strongly emissive fluorescein.

I. Change in viscosity of suspended squalene aerosol with exposure to hydroxyl radicals

Fig. S10 compares the change in viscosity of deposited and suspended squalene aerosol as oxidised by $\cdot\text{OH}$. Because of the sensitivity of the droplets to FLIM laser exposure, a few tests were carried out with minimal exposure. Fig S10B shows a set of droplets measured over a series of images, four single decays and one single end-point measurement.

A change in viscosity from ~ 60 to 500 mPa s was measured for both the cover-slide and trapping experiments upon the OH exposure.

The fact that there is no difference in the final viscosity of the oxidised material between the trapped and deposited droplets can be contrasted with the ozonolysis experiment, where a large change in morphology was observed. This result could be due to the formation of generally lower volatility products compared to ozonolysis, i.e. alcohols rather than aldehydes. Therefore removing the slide contact and measuring smaller particles in the trapping experiments does not affect the final viscosity.

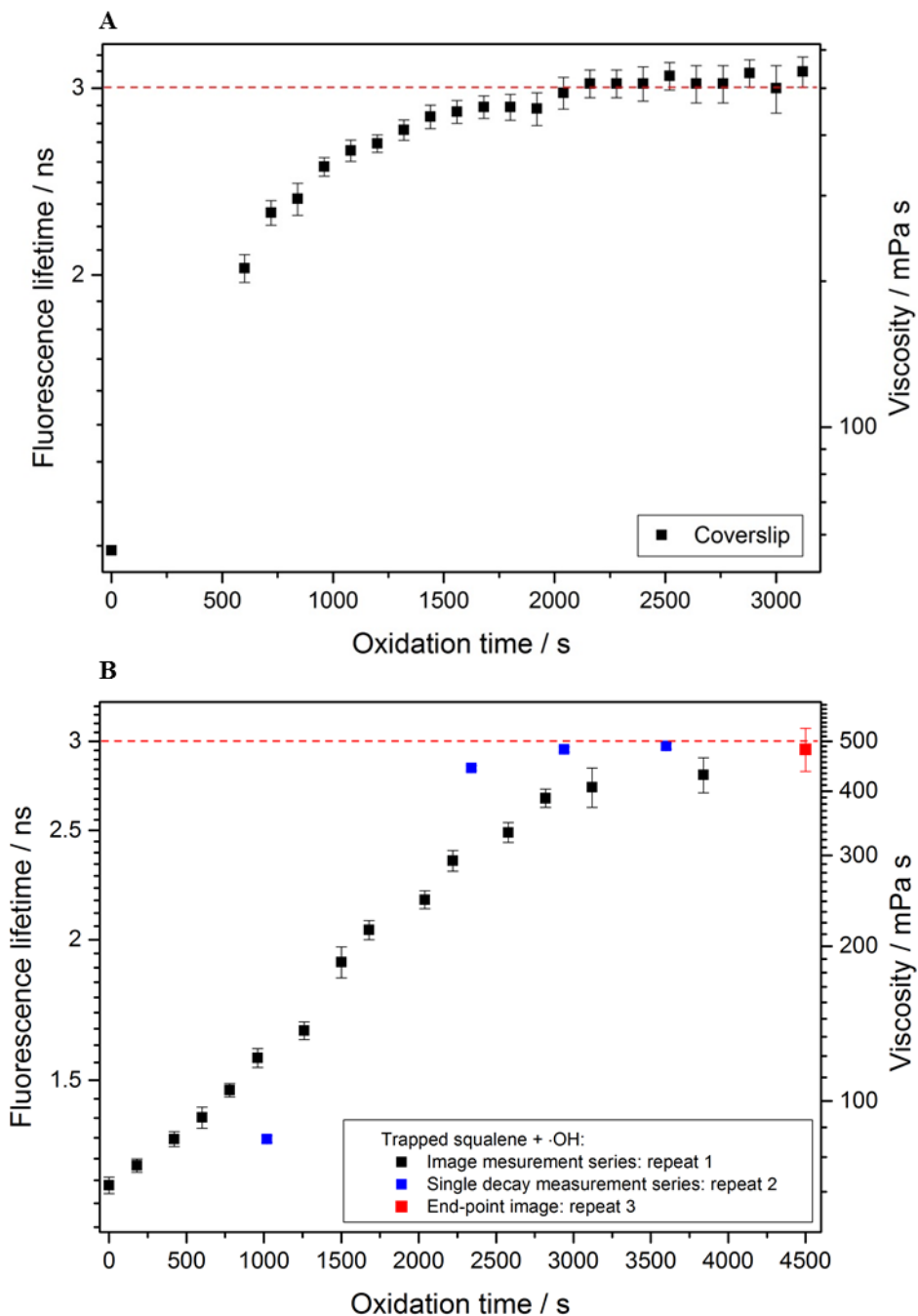


Fig. S10. Change in viscosity of squalene aerosol with exposure to $\cdot\text{OH}$. **A:** Oxidation of squalene droplets on a cover-slide. **B:** Optically trapped squalene aerosol (black squares). Red dotted line indicates the approximate viscosity after complete oxidation (~ 500 mPa s). Repeat 1: Image series (on average 200 s/image); repeat 2: four single decays (10 seconds collection per decay); repeat 3: end-point value (80 s image).

J. Comparison of oxidation products between ozonolysis and oxidation by OH radicals

According to the FLIM viscosity measurements, there is a different end-point viscosity due to oxidation by ozone or hydroxyl radicals. An approximate end-point of 5000 mPa s was measured for ozone (and this value is the lower estimate since the lifetime of Bodipy-C₁₀ in fully oxidised squalene was at the far end of the rotor calibration range, reducing the reliability in measured viscosity, see Figure S2) and only 500 mPa s for ·OH. To investigate whether the mass spectra of the two sets of chemical products can provide an insight into why this was, the carbon oxidation state for each peak in the two mass spectra, for which an elemental formula could be assigned was calculated and plotted against the carbon number of the same compound for the *m/z* range 100-2000. Fig. S11 shows this data for both oxidation pathways.

Fig. S11 shows that there is minimal difference in the number of carbon atoms in the molecules in both oxidised mixtures. The shape of the distribution is very similar. However the distribution for the ·OH oxidation is very significantly shifted to lower oxidation states. Therefore, in general the mixture oxidised with OH is less oxidised than for ozone oxidation. This can be explained by the reaction conditions of the OH oxidation reactions, which took place in a N₂ atmosphere preventing the usual peroxy radical chemistry leading to highly oxidized products during OH oxidation in air. In contrast, in ozonolysis, mainly oxidised non-volatile species are produced such as carboxylic acids, aldehydes and peroxides. Therefore, the larger viscosity for ozonolysed squalene can be attributed to greater dipole-dipole intermolecular bonding, reducing the mobility within the mixture and increasing the viscosity.

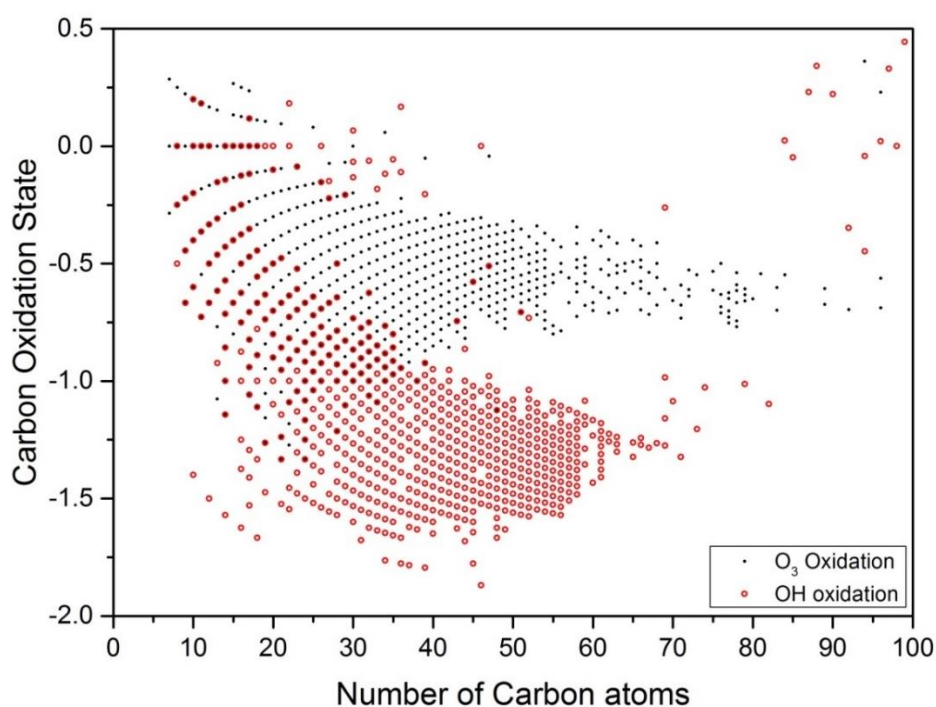


Fig. S11. Carbon oxidation state for squalene oxidation by ozone (black circles) and ·OH (red open circles), plotted against carbon number, for *m/z* 100-2000. Each data point corresponds to a peak in the mass spectra for which an elemental composition could be assigned.

K. Brightfield images of $\cdot\text{OH}$ oxidised squalene/Bodipy-C10 particles

To confirm that the $\cdot\text{OH}$ oxidised squalene particles were indeed in a liquid state after oxidation, the droplets were left to react for more than 2 hours and then released on the coverslip in order to study their morphology. The observed brightfield images (Fig. S12) revealed that the droplets were still liquid by their spreading over the coverslip, thus concluding that viscosity did not increase as dramatically as was the case with the ozone oxidation.

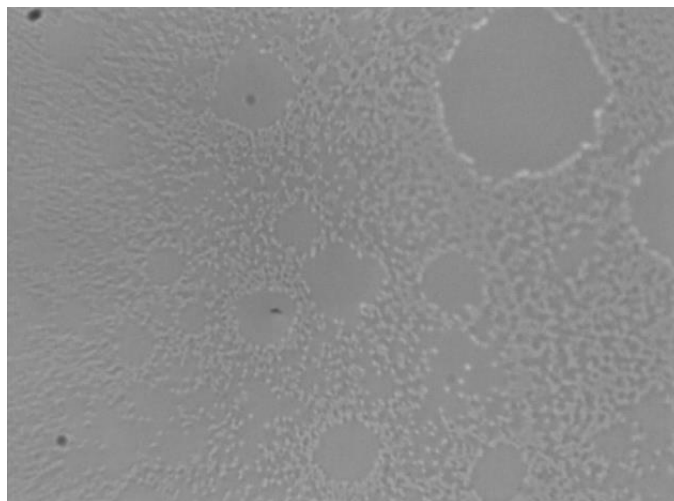


Fig. S12. Brightfield image of a squalene droplet deposited onto the cover-slide after complete oxidation with $\cdot\text{OH}$ in the trap.

L. Effect of oxidant gases on squalene aerosol

It was considered that during the oxidation experiments the UV lamp might not convert all of the oxygen into ozone or H_2O_2 into $\cdot\text{OH}$. These gas-phase species may cause a background change in fluorescence lifetime. Therefore two controls were carried out to observe the effect of oxygen and H_2O_2 vapour on the fluorescence lifetime of the trapped squalene/Bodipy- C_{10} aerosol, by repeating the experiments with the lamp off.

Fig. S13 shows the changing fluorescence lifetime of the aerosol with exposure to the two species. Also included in Fig. S13 are two example end-points of the lifetime change when exposed to ozone and $\cdot\text{OH}$. Although in both cases some increase in lifetime was measured when exposed to oxygen (A) and H_2O_2 vapour (B), the change is less than the change measured when oxidised with ozone or $\cdot\text{OH}$, i.e. 1.5 compared to 5 ns in the case of oxygen/ozone and 1.3 compared to 3 ns in the case of $\text{H}_2\text{O}_2/\cdot\text{OH}$. It is also probable that, even though FLIM laser exposure was kept to a minimum in these tests, some degradation, and therefore lifetime increase, might be due to laser exposure.

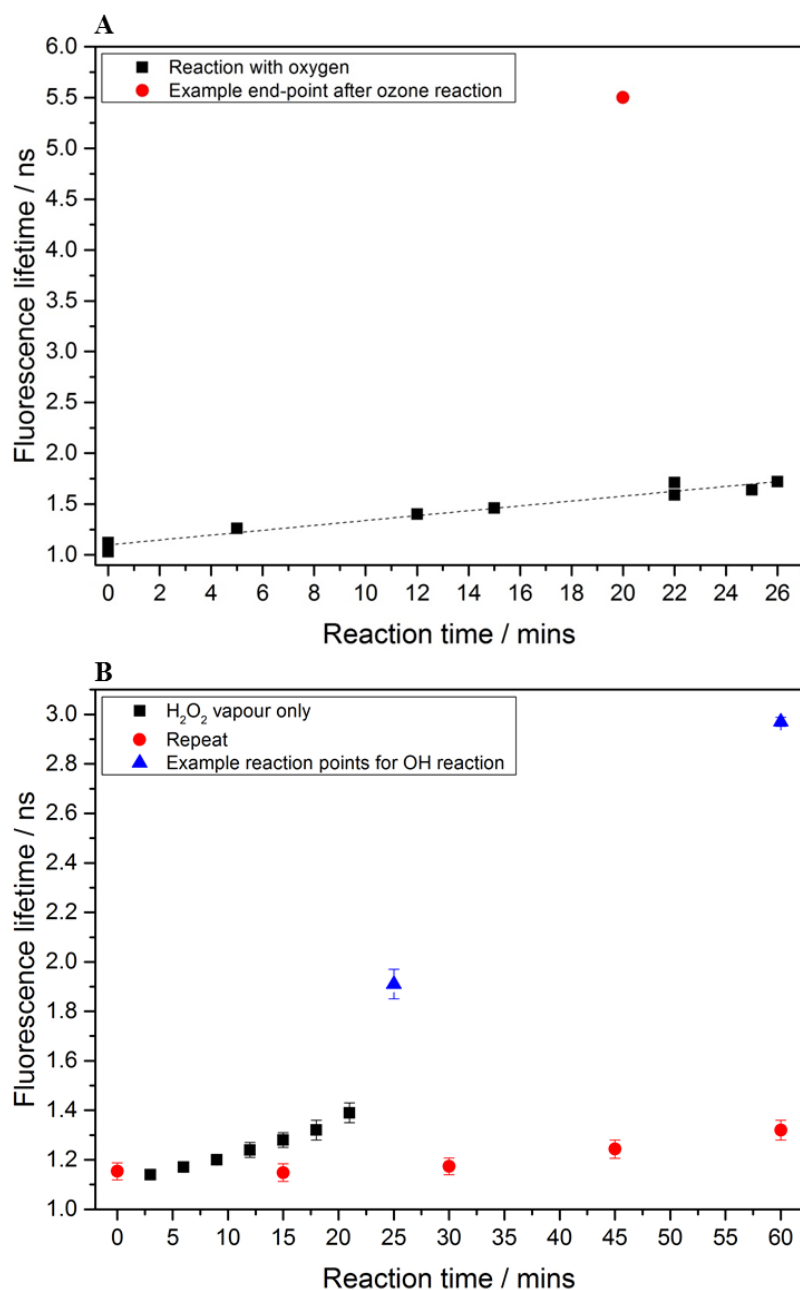


Fig. S13. Effect on fluorescence lifetime of trapped squalene/Bodipy-C₁₀ aerosol when exposed to A) oxygen, to account for background change in ozone experiment and B) H₂O₂ vapour, to account for background change in ·OH experiment. Each plot includes an example end-point value from the ozone and ·OH experiments.

M. Absorption spectrum of squalene

In order to investigate likely absorption of the trapping laser wavelength (1064 nm) by the trapped particles, UV-Vis absorption measurements were taken of bulk squalene with and without the Bodipy-C₁₀ rotor (Fig. S14). It can be seen that any absorption of the trapping wavelength is below the detection limit and therefore it is expected that there was a negligible heating effect from the trapping laser on the trapped particles.

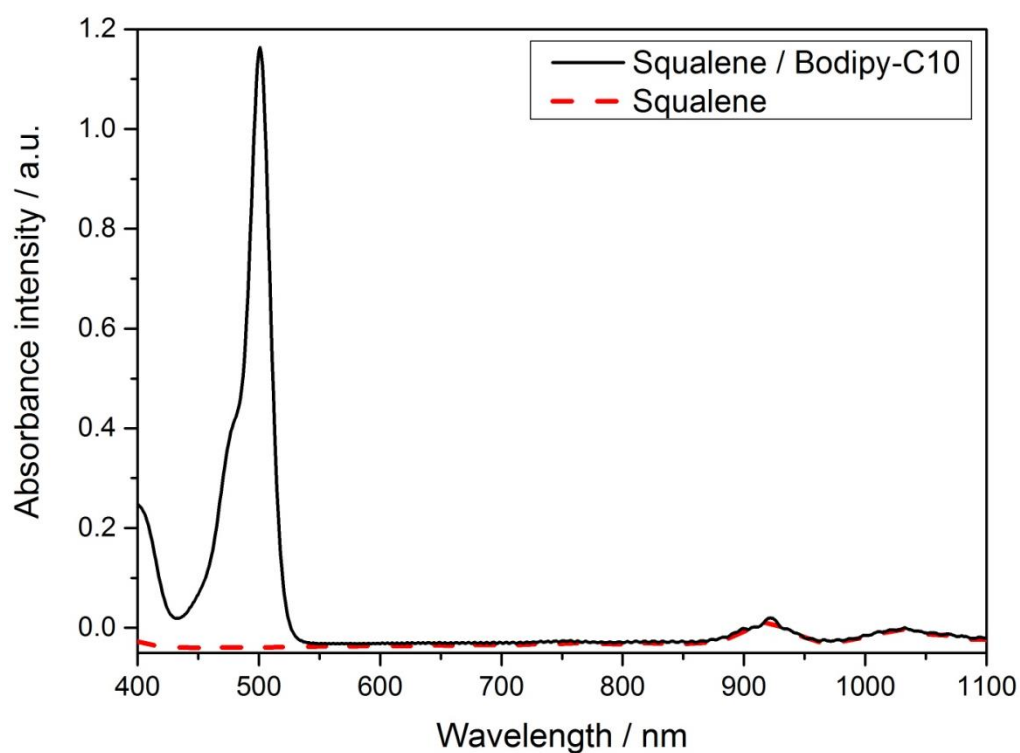


Fig. S14: UV-Vis absorption spectrum of pure squalene (red dashed line) and squalene with Bodipy-C₁₀ (20 μ m) (black line).

N. Effect of FLIM laser exposure on the fluorescence lifetime

For the two-photon excitation (TPE) experiments on deposited squalene droplets, laser powers were kept <4.5 mW at the sample. This resulted in no significant drift in lifetime over at least 55 minutes of imaging compared to the lifetime change induced by the oxidation of squalene (Fig. S15). An image size of 128x128 pixels was used. The ADC was set to 256 and image acquisition times were ~200 seconds.

In the case of the single photon excitation (SPE) trapping squalene/Bodipy-C₁₀ oxidation experiments, the effect of FLIM laser exposure was harder to constrain. In particular, the fluorescence lifetime was very sensitive to exposure and the effect could be quite variable between repeated tests. Fig S15 shows the change in fluorescence lifetime of squalene/Bodipy-C₁₀ aerosol trapped in N₂ when exposed to the FLIM laser. The change in lifetime ranged from 1.1 to 2 ns after 14 minutes exposure, to just 0.2 ns after 22 minutes. These effects were more problematic for the ·OH tests, since the experiments took longer and signal intensity was more difficult to maintain due to additional loss of the dye from attack by ·OH. Therefore longer collection times/higher laser powers were needed. Since it was difficult to control the effect of the FLIM laser, it was important for each repeat of the squalene oxidation experiments to take end-point measurements that had undergone minimal laser exposure for comparison.

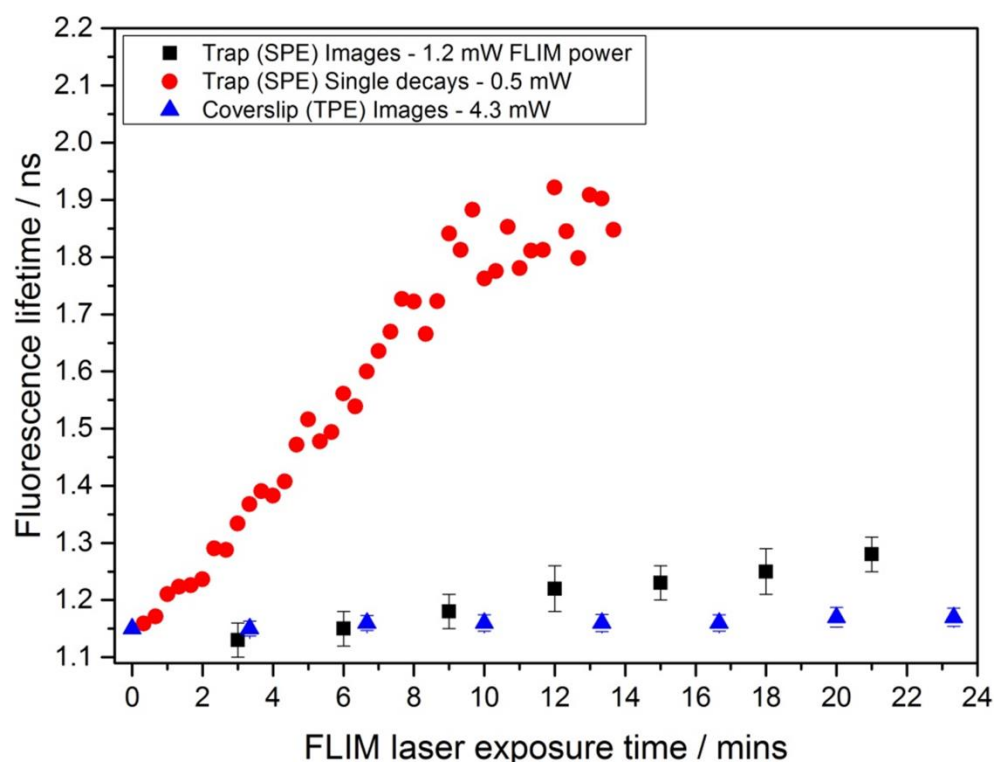


Fig. S15. Repeat exposure tests of FLIM laser on fluorescence lifetime of squalene/Bodipy-C₁₀ aerosol, trapped in N₂ flow. Black squares: SPE (490 nm) image series; Red circles: SPE single decay series; Blue triangles: test from cover-slide experiments on TP set-up.

O. References

- 1 Y. Wu, M. Štefl, A. Olzyńska, M. Hof, G. Yahioglu, P. Yip, D. R. Casey, O. Ces, J. Humpolíčková and M. K. Kuimova, *Phys. Chem. Chem. Phys.*, 2013, **15**, 14986.
- 2 M. R. Dent, I. López-Duarte, C. J. Dickson, N. D. Geoghegan, J. M. Cooper, I. R. Gould, R. Krams, J. A. Bull, N. J. Brooks and M. K. Kuimova, *Phys. Chem. Chem. Phys.*, 2015, **17**, 18393–402.
- 3 M. K. Kuimova, *Phys. Chem. Chem. Phys.*, 2012, **14**, 12671–86.
- 4 N. Hosny, G. Mohamedi, P. Rademeyer, J. Owen, Y. Wu, M. Tang, R. Eckersley, E. Stride and M. Kuimova, *Proc. Natl. Acad. Sci. U. S. A.*, 2013, **110**, 9225–30.
- 5 C. Giorio, E. Moyroud, B. Glover, P. Skelton and M. Kalberer, *Anal. Chem.*, 2015, **87**, 9900–9907.
- 6 Y. Hua and D. Jenke, *J. Chromatogr. Sci.*, 2012, **50**, 213–227.
- 7 L. Renbaum-Wolff, J. W. Grayson, A. P. Bateman, M. Kuwata, M. Sellier, B. J. Murray, J. E. Shilling, S. T. Martin and A. K. Bertram, *Proc. Natl. Acad. Sci. U. S. A.*, 2013, **110**, 8014–9.
- 8 A. Greer and J. Liebman, *The Chemistry of Peroxides. Volume 3. Part 1.*, John Wiley & Sons, Ltd., 2014.